Lorenz energy cycle of the global atmosphere based on reanalysis datasets

Liming Li,[1] Andrew P. Ingersoll,[1] Xun Jiang,[1] Daniel Feldman,[1] and Yuk L. Yung[1]

Received 12 March 2007; revised 10 July 2007; accepted 25 July 2007; published 24 August 2007.

[1] The mean state of the global atmospheric energy cycle is re-examined using the two reanalysis datasets — NCEP2 and ERA40 (1979–2001). The general consistency between the two datasets suggests that the present estimates of the energy cycle are probably the most reliable ones. The comparison between the present and a previous study shows noticeable discrepancies in some of the energy components and conversion rates. The current estimate of the transformations from mean potential energy to mean kinetic energy $C(P_M, K_M)$ further suggests that the near-surface processes play an important role in the conversion rate $C(P_M, K_M)$, along with the Ferrel cell and Hadley cells, which probably change the direction of the conversion rate $C(P_M, K_M)$. **Citation:** Li, L., A. P. Ingersoll, X. Jiang, D. Feldman, and Y. L. Yung (2007), Lorenz energy cycle of the global atmosphere based on reanalysis datasets, *Geophys. Res. Lett.*, *34*, L16813, doi:10.1029/2007GL029985.

1. Introduction

[2] The Lorenz atmospheric energy cycle describes the general circulation from a perspective that emphasizes energy transformation – how the incoming solar radiation generates potential energy that is transferred to kinetic energy and is finally lost to frictional dissipation. These statistical characteristics of the global atmospheric energy cycle are useful for the validation of general circulation models since they constitute constraints that must be fulfilled. Most of the earlier computations of the energetics of the atmosphere are based on data sets that do not cover the area south of 20°N [*Krueger et al.*, 1965; *Wiin-Nielsen*, 1967; *Peixoto and Oort*, 1974; *Oort and Peixoto*, 1974, 1976; *Sheng and Hayashi*, 1990; *Hu et al.*, 2004]. The only previous study that covered the globe [*Oort*, 1983] was based on a 10-year (1963–1973) rawinsonde dataset with observational limitations due to the sparseness of stations in the Southern Hemisphere (SH) and large data gaps at some stations due to adverse meteorological conditions.

[3] The National Centers for Environmental Prediction — National Center for Atmospheric Research (NCEP-NCAR) and the European Center for Medium-Range Weather Forecasts (ECMWF) have produced retroactive records of more than 40 years of global atmospheric fields with a quality not available heretofore [*Kalnay et al.*, 1996; *Kanamitsu et al.*, 2002; *Uppala*, 2001; *Uppala et al.*, 2005]. The two reanalysis datasets (NCEP2 and ERA40), which are produced by an advanced data assimilation system using numerical models based on the modern observational data, have improved in several aspects compared with the old datasets used in the previous study [*Oort*, 1983]. Firstly, the two reanalysis datasets between 1979 and 2001 are satellite-based datasets, whose quality is better than that of the old dataset before 1979 [*Oort*, 1983]. Secondly, more observable variables in the two reanalysis datasets make it possible to compute directly the conversion rate $C(P_E, K_E)$, which is estimated indirectly in the previous study [*Oort*, 1983]. Thirdly, the domain of the two reanalysis datasets covers the whole globe in the meridional direction (90°S–90°N) and includes the troposphere and middle stratosphere (1000 mbar–10 mbar), and so is larger than the domain of old datasets (80S–80N and 1000 mbar–50 mbar). The polar regions and middle stratosphere, which are missing from the old datasets [*Oort*, 1983], are important because stratospheric jets contribute to the mean kinetic energy and the polar regions affect the mean potential energy by changing the global mean temperature. Fourthly, the horizontal spatial resolution of the two reanalysis datasets ($2.5° \times 2.5°$) is much finer than the irregular spatial resolution in the old datasets (less than 1000 stations in the global domain). Finally, the advanced data assimilation methods make the reanalysis datasets physically consistent and uniform, hence markedly improved from the old datasets which contained many gaps in time and space [*Oort*, 1983]. It should be mentioned that some potential biases are introduced into the reanalysis datasets during the process of data assimilating when we notice that the reanalysis datasets have superiorities in density, continuity, and quality of observation and physical consistency and uniformity of data.

2. Methodology

[4] Following the formulation by *Lorenz* [1955] and the notation used by *Peixoto and Oort* [1974], we calculate the following terms in the energy cycle in the mixed space-time domain based on the two datasets (NCEP2 and ERA40): the mean available potential energy P_M, the eddy available potential energy P_E, the mean kinetic energy K_M, the eddy kinetic energy K_E, the conversion rate between the mean kinetic energy and available potential energy $C(K_M, P_M)$, the conversion rate between the mean and eddy available potential energies $C(P_M, P_E)$, the conversion rate between the eddy available potential energy and kinetic energy $C(P_E, K_E)$, and the conversion rate between the eddy and mean kinetic energies $C(K_E, K_M)$. Most of the computations are based on geopotential height, zonal wind, meridional wind, and temperature. These variables have the highest data quality rating in the two reanalysis datasets [*Kalnay et al.*, 1996; *Uppala*, 2001; *Uppala et al.*, 2005]. The only variable with relatively low data quality — pressure vertical

[1]Division of Geological and Planetary Sciences, California Institute of Technology, Pasadena, California, USA.

0094-8276/07/2007GL029985

Table 1. Global Integrals of the 23-Year Mean Energy Cycle Based on Monthly Evaluation of the Two Reanalysis Datasets NCEP2 and ERA40 (1979–2001)

	Global		NH		SH		
	NCEP2	ERA40	NCEP2	ERA40	NCEP2	ERA40	Unit
P_M	42.5	43.2	39.3	40.2	46.7	47.1	10^5 J/m^2
P_E	5.0	5.5	6.3	6.5	3.9	4.7	10^5 J/m^2
K_M	7.7	7.8	5.9	5.9	9.9	10.1	10^5 J/m^2
K_E	6.2	6.6	6.6	6.6	6.0	6.8	10^5 J/m^2
$C(P_M, P_E)$	1.69	1.79	1.58	1.52	1.88	2.15	W/m^2
$C(P_E, K_E)$	2.38	2.01	2.23	1.76	2.62	2.31	W/m^2
$C(K_E, K_M)$	0.34	0.20	0.29	0.17	0.40	0.24	W/m^2
$C(P_M, K_M)$	0.17	0.05	0.16	0.19	0.19	−0.08	W/m^2
$G(P_M)$[a]	1.85	1.84	1.74	1.71	2.07	2.07	W/m^2
$G(P_E)$[a]	0.69	0.22	0.65	0.24	0.74	0.16	W/m^2
$D(K_M)$[a]	0.51	0.25	0.45	0.36	0.59	0.16	W/m^2
$D(K_E)$[a]	2.04	1.81	1.94	1.59	2.22	2.07	W/m^2

[a]Values of generating terms ($G(P_M)$ and $G(P_E)$) and dissipation terms ($D(P_M)$ and $D(P_E)$) are indirectly estimated by assuming a balance exists between the input terms and output terms for each energy component. Global integrals are calculated by weighting the zonal-mean energy components and conversion rates in the meridional direction by cosine of latitude and in the vertical direction by the different intervals of pressure levels. A multiplication factor [*Oort*, 1983], which takes into account the mean mass distribution over the globe (e.g., less mass over the mountains), is also used for the global integrals.

velocity ω — is used in some terms of the conversion rates $C(P_M, P_E)$ and $C(K_E, K_M)$. Our calculation indicates that these terms involving ω are roughly one order of magnitude smaller than the other terms in $C(P_M, P_E)$ and $C(K_E, K_M)$. To take advantage of the higher data quality of horizontal velocity in datasets, the terms involving the vertical velocity in the other two conversion rates $C(P_M, K_M)$ and $C(P_E, K_E)$ were transformed into terms involving horizontal velocity using the continuity equation [*Peixoto and Oort*, 1974]. The generation rates of the mean and eddy potential energies $G(P_M)$ and $G(P_E)$, and dissipation rates of the mean and eddy kinetic energies $D(K_M)$ and $D(K_E)$ are evaluated by balancing the corresponding conversion rates.

[5] The synoptic eddies (cyclones and anticyclones), with length-scale around a thousand kilometers and time-scale of several days, play an important role in the atmospheric energy cycle. In this paper, the eddies with sizes and lifetimes smaller than the spatial and temporal resolutions of the daily data of the two reanalysis datasets (~250 km at the equator and 1 day) are treated in the category of molecular motions [*Lorenz*, 1955]. Most of the synoptic eddies have lifetime less than one month, hence we present a monthly evaluation of the parameters that characterize the energy cycle based on the daily data, in which the transient eddy component contains only eddies with time scales less than a month. However, the yearly evaluation of the energy cycle, in which the transient eddy component is defined as eddies with all time scales less than 12 months, is presented in the auxiliary material[1] to facilitate comparison of our results with the previous results based on the yearly evaluation of 10-year rawinsonde observations [*Oort*, 1983]. The monthly evaluation, which is missing in the previous study [*Oort*, 1983], is emphasized in this study, for the following reasons: (1) The monthly evaluation is a more suitable evaluation than the yearly evaluation when considering the time-scale of cyclone/anticyclone activity. (2) The monthly evaluation can be utilized to discuss the annual and seasonal characteristics of the energy cycle. (3) In order to better resolve the roles of large-scale meridional circulations (the Hadley cell and the Ferrel cell), the monthly evaluation is a better choice than the yearly evaluation (see the discussion in section 3).

3. Results

3.1. Monthly Evaluation

3.1.1. Global Integrals

[6] Table 1 presents the 23-year (1979–2001) mean state of the global integrals of energy cycle based on the monthly evaluation of the NCEP2 and ERA40. The discrepancies of the energy components (P_M, P_E, K_M, and K_E) between the two reanalysis datasets are smaller than 10% in the global scale. The spatial patterns of the energy components are also similar between the two datasets (Figure 1). The discrepancies of the conversion rates $C(P_M, P_E)$ and $C(P_E, K_E)$ between the two reanalysis datasets are smaller than 15%, and the other two conversion rates $C(K_E, K_M)$ and $C(P_M, K_M)$ display relatively larger discrepancies between the two reanalysis datasets. Table 1 also shows that the estimates from the two reanalysis datasets both are positive for the conversion rate $C(P_M, K_M)$ in the global scale. The yearly evaluation of the conversion rate $C(P_M, K_M)$ (Table S3 in the auxiliary material) has different signs with absolute value 0.06 W/m^2, which is much smaller than the magnitude in the previous study with value −0.15 W/m^2 [*Oort*, 1983]. Furthermore, the comparison between the monthly evaluation (Figure 2) and the yearly evaluation (Figure S5 in the auxiliary material) shows that the positive centers of $C(P_M, K_M)$ corresponding to the Hadley cell in the troposphere of both hemispheres (20° and 200 mbar) based on the yearly evaluation are much smaller than the corresponding positive centers based on the monthly evaluation. The yearly evaluation underestimates the Hadley cell because the yearly-mean meridional velocity and temperature conceal the equatorward motion and high temperature in summer and the poleward motion and cold temperature in winter for the two hemispheres. Therefore, it is better to use monthly evaluation to estimate the conversion rate $C(P_M, K_M)$ in order to realistically resolve the large-scale meridional circulation. The monthly evaluation (Figure 2) also shows that the negative centers (50° and 200 mbar) corresponding to the Ferrel cell are bigger and stronger than the positive centers (20° and 200 mbar) corresponding to the Hadley cell, which is consistent with the previous study [*Oort*, 1983]. Figure 2 also shows near-surface maxima of the conversion rate in the southern hemisphere, which correspond to the heat-driven circulation. The contribution from the strong maxima associated with the near-surface processes is larger than the net contribution from the Ferrel cell and the Hadley cell so that the global integral of $C(P_M, K_M)$ based on the monthly evaluation is positive. The positive sign of $C(P_M, K_M)$ based on the monthly evaluation of the two reanalysis datasets is probably real because the conversion rate $C(P_M, K_M)$ is closely tied with the mean meridional velocity and temperature, which have the highest

[1]Auxiliary material data sets are available at ftp://ftp.agu.org/apend/gl/2007gl029985. Other auxiliary material files are in the HTML.

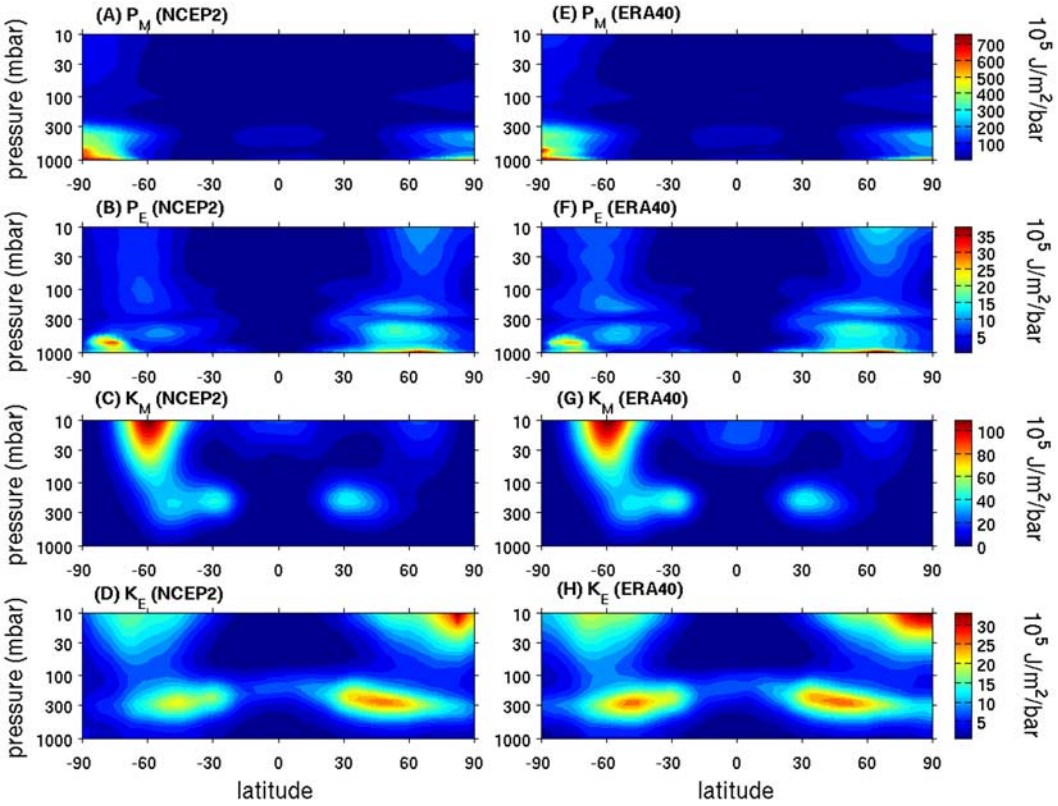

Figure 1. 23-year mean energy components in latitude-altitude cross section based on the monthly evaluation of the two reanalysis datasets (NCEP2 and ERA40)The four energy components (a)P_M, (b)P_E, (c)K_M, and (d)K_E based on NCEP2. (e, f, g, h) The corresponding energy components based on ERA40.

data quality in the two reanalysis datasets. In summary, our estimates based on the two reanalysis datasets support the previous conclusion [*Oort*, 1983] that the Ferrel cell is more important than the Hadley cell in the transformations from the mean potential energy P_M to the mean kinetic energy K_M. The current estimates further suggest that the near-surface processes probably change the direction of the conversion rate $C(P_M, K_M)$ in the global scale.

3.1.2. Three-Dimensional Structures

[7] Figure 1 displays the structure of energy components in vertical cross section based on the monthly evaluation of the two reanalysis datasets. Figure 1 shows that the two reanalysis datasets agree with each other very well. The maxima of P_M are located near the surface around the two poles, which are associated with the greatest temperature departures from the global mean in these regions. The structure of P_E is affected by the pattern of P_M with a slight displacement to the equator. The maxima of K_M in the mid-latitudes of the troposphere and stratosphere are linked to the tropospheric and stratospheric jets. The stratospheric maximum of K_M in the Southern Hemisphere (SH) is much stronger than that in the Northern Hemisphere (NH) because the center of the stratospheric jet in the NH is located above 10mbar. The structure of K_E is associated with the pattern of K_M with a slight displacement to the poles. In general, the eddy kinetic energy K_E is also affected by the eddy potential energy P_E because the synoptic cyclones are controlled by the temperature perturbations. The maxima of K_E are between the centers of K_M and P_E, which suggests that the structure of K_E is the result of a balance between K_M and P_E.

[8] The global distribution of the eddy potential energy and eddy kinetic energy (P_E and K_E), which are integrated in the vertical direction for each grid-point, is given in the auxiliary material Figure S1. The two reanalysis datasets both show that the maxima of P_E in the NH are over the coasts of Asia and North America. The maxima of P_E in the SH are near the boundary of Antarctica. The distribution of P_E suggests that the land-sea temperature contrast must play an important role in the eddy potential energy P_E. The maxima of K_E in the NH are associated with the two storm tracks over the Pacific and Atlantic oceans [*Harnik and Chang*, 2003]. A belt of maximum contribution to K_E in the mid-latitudes of the SH is related to the storm tracks over the Southern Ocean (SO) [*Trenberth*, 1991].

[9] Figure 2 shows the structure of conversion rates in vertical cross section. Both datasets show that the maxima of $C(P_M, P_E)$ are located in the mid-latitudes of the lower troposphere in both hemispheres, which are associated with the mid-latitude cyclone activity. The maxima of $C(P_E, K_E)$ are found near the surface around South Pole (SP), and are associated with heat-driven rising and sinking motions over the Antarctica. The structure of $C(K_E, K_M)$ shows that the maxima shift to the equator while the minima shift to the poles relative to the positions of jet streams in the troposphere and stratosphere. The maxima and minima of $C(P_M, K_M)$ in the free troposphere are associated with the direct

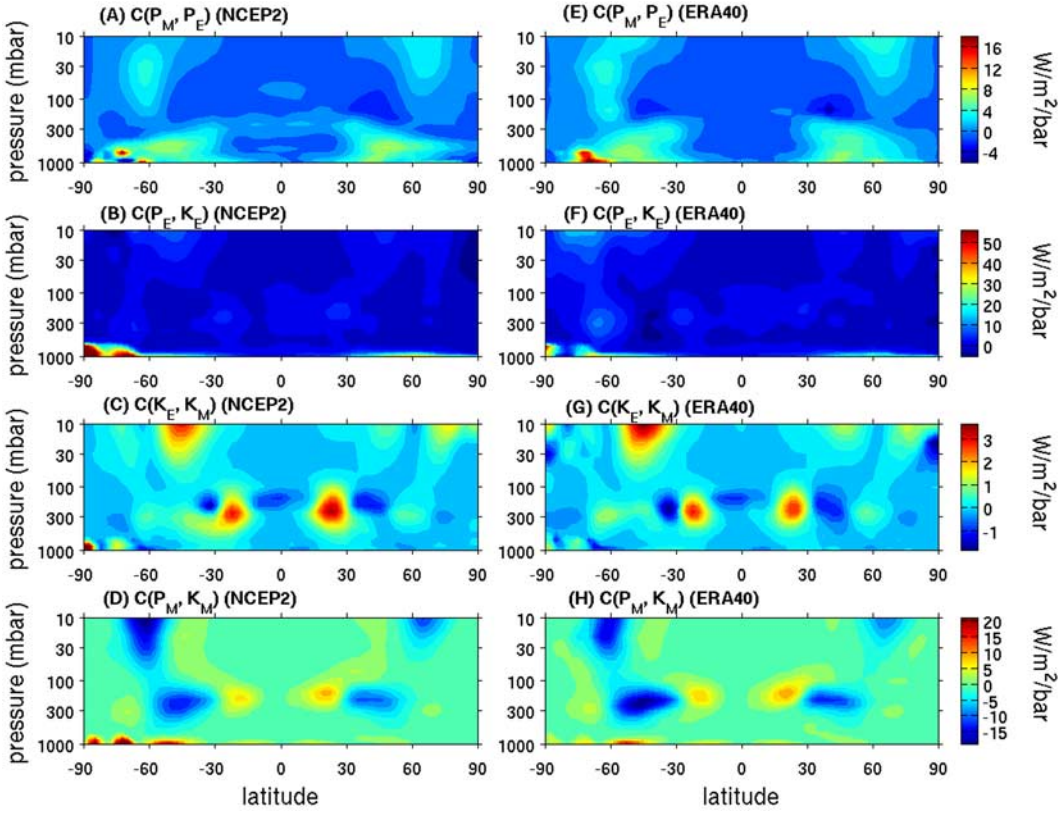

Figure 2. 23-year mean conversion rates in latitude-altitude cross section based on the monthly evaluation of the two reanalysis datasets (NCEP2 and ERA40). Conversion rates (a) $C(P_M, P_E)$, (b) $C(P_E, K_E)$, (c) $C(K_E, K_M)$, and (d) $C(P_M, K_M)$ based on NCEP2. (e, f, g, h) The corresponding conversion rates based on the ERA40.

Hadley cell ($C(P_M, K_M) > 0$) and the indirect Ferrel cell ($C(P_M, K_M) < 0$). The calculation of $C(P_M, K_M)$ in the free troposphere (between 700mbar and 100mbar) shows that the net $C(P_M, K_M)$ from the Ferrel cell and Hadley cell is about -0.39 W/m^2 for NCEP2 and -0.36 W/m^2 for ERA40. Figure 2 also shows that the near-surface (between 1000 mbar and 700 mbar) processes, corresponding to the heat-driven circulation, play an important role in the $C(P_M, K_M)$ (0.54 W/m^2 and 0.43 W/m^2 for NCEP2 and ERA40, respectively). The near-surface maxima of $C(P_M, K_M)$ in the SH are stronger in NCEP2 than in ERA40 (0.41 W/m^2 vs. 0.30 W/m^2 for NCEP2 and ERA40, respectively).

[10] Figure S2 in the auxiliary material displays the global distribution of the conversion rate $C(P_E, K_E)$. The two reanalysis datasets both show that the conversion rate $C(P_E, K_E)$ has roughly same spatial patterns with the eddy kinetic energy P_E (Figure S1 in the auxiliary material), which suggests that the direct circulation driven by the land-sea temperature contrast also play an important role in the transformation of the eddy potential energy P_E to the eddy kinetic energy K_E.

3.1.3. Seasonal Variations

[11] The seasonal cycles in both hemispheres based on the monthly evaluation of the two reanalysis datasets are given in Tables S1 and S2 in the auxiliary material. Table S1 shows that the energy components and conversion rates in the NH have their maximum values in winter except for the conversion rate $C(K_E, K_M)$ from the ERA40, which is probably somewhat underestimated. Table S1 also shows that all energy components and conversion rates in the NH have their minimum values in summer. Particularly, the two reanalysis datasets both indicate that the conversion rate $C(P_M, K_M)$ in the NH is negative in summer. The negative $C(P_M, K_M)$ suggests that the mean kinetic energy K_M is converted to the man potential energy P_M in summer in the NH, which is different from the transformations in the other seasons. Both datasets show that the energy components in the SH (Table S2) have their maximum values in winter except for P_E, which has its maximum values in spring. All energy components in the SH have minimum values in summer. The estimate in the SH based on the NCEP2 shows that all conversion rates have their maximum values in summer and their minimum values in winter except for $C(P_M, K_M)$. However, the estimate in the SH based on the ERA40 shows more complicated seasonal cycles for these conversion rates. The big discrepancies of the conversion rates in the SH on the seasonal time scale between the NCEP2 and ERA40 are probably due to the relatively limited observations in the SH and different data assimilation techniques between the two datasets.

3.2. Yearly Evaluation

[12] Table S3 in the auxiliary material presents the global integrals of energy cycle based on the yearly evaluation of the two reanalysis datasets. Table S3 shows that the eddy energies P_E and K_E are larger in the yearly evaluation than in the monthly evaluation, and the mean energies P_M and K_M are smaller in the yearly evaluation than in the monthly

evaluation. Table S3 also shows that the SH has larger P_M and K_M, and smaller P_E and K_E compared with the NH, which is consistent with the previous estimate [*Oort*, 1983]. The yearly evaluation based on NCEP2 and ERA40 shows the mean energies P_M and K_M have values of 37.1×10^5 J/m^2 and 6.5×10^5 J/m^2 respectively, which are larger than the results from the 10-year rawinsonde dataset with values of 33.3×10^5 J/m^2 and 4.5×10^5 J/m^2 respectively [*Oort*, 1983]. The discrepancies between the current and previous estimates [*Oort*, 1983] probably arise because the two reanalysis datasets used in the current estimates extend to polar regions including the coldest latitudes (80°–90°) and higher altitudes including the region of strong jets in the middle stratosphere, which are not covered in the previous rawinsonde observations [*Oort*, 1983]. The comparison of yearly evaluation between this study and the previous study [*Oort*, 1983] also shows noticeable discrepancies in the conversion rates. We think that the current estimates of the conversion rates are more reliable, considering the higher data quality of the two reanalysis datasets and the fact that some of the conversion rates in the previous study are estimated indirectly [*Oort*, 1983].

[13] The structure of energy components in the vertical cross section based on the yearly evaluation is given in Figure S3 in the auxiliary material. The two reanalysis datasets show that the yearly evaluation of the mean energies P_M and K_M have almost the same spatial patterns as the monthly evaluation, but the yearly evaluation of eddy energy components P_E and K_E show significant discrepancies with the monthly evaluation. The yearly evaluation (Figure S3) shows that the stratospheric maxima of P_E appear in the polar regions, which replace the tropospheric maxima in middle and high latitudes based on the monthly evaluation (Figure 1). The stratospheric maxima of P_E in the polar regions suggest that the temperature perturbation in a time-scale between 1 month and 1 year is dominant in these regions. In the case of the eddy kinetic energy K_E, the yearly evaluation shows that the stratospheric maxima in both hemispheres are slightly displaced toward the equator compared with the monthly evaluations. In addition, the yearly evaluation shows that the stratospheric maxima of K_E are stronger in the SH than in the NH, which is different from the monthly evaluation in which the stratospheric maxima of K_E are stronger in the NH than in the SH. However, these discrepancies of P_E and K_E between the monthly evaluation and yearly evaluation have negligible effect on the vertical-integrating of P_E and K_E because of the small mass weighting of the stratosphere. Therefore, the global distribution of P_E and K_E based on the yearly evaluation (Figure S4) shows almost the same patterns as the ones based on monthly evaluation (Figure S1).

[14] The structure of conversion rates based on the two reanalysis datasets displays surprising agreement between the yearly and monthly evaluations (Figures 2, S2, S5, and S6), which suggests that different time scales do not affect these correlations appearing in the conversion rates.

4. Conclusions

[15] The classical Lorenz energy cycle of the global atmosphere is updated based on the monthly and yearly evaluation of two reanalysis datasets (NCEP2 and ERA40). The general consistency of the global integrals, three-dimensional structure, and seasonal variations between the two datasets suggest that the present estimates of the global atmospheric energetics are the most reliable ones. The comparison of the yearly evaluation between this study and the previous study [*Oort*, 1983] shows some noticeable discrepancies in the energy components and conversion rates, but the energetics of the global atmosphere based on the two reanalysis datasets supports the classical process of the energy cycle suggested by *Lorenz* [1955] and *Oort* [1983]: $P_M \rightarrow P_E \rightarrow K_E \rightarrow K_M$. However, the current estimates suggest that the near-surface processes play an important role in the transformations from the mean potential energy to mean kinetic energy so that the mean kinetic energy P_M is converted to the mean potential energy K_M in the global scale, which is different from the results based on the yearly evaluation of old datasets [*Oort*, 1983].

[16] Our calculations also suggest that the time evolution of global atmospheric energy cycle (not shown) has significantly different, even opposite, trends for some energy components and conversion rates between the two reanalysis datasets, even though the 23-year mean state of the energy cycle based on the two reanalysis datasets has general agreement. The trend of the global atmospheric energy cycle and its validation are beyond the scope of this paper, and will be addressed in future work. In addition, the interesting relationship of locations between the mean kinetic energy K_M and the conversion rate $C(K_E, K_M)$, which has an important application to the jet migration, also needs to be discussed further.

References

Harnik, N., and E. K. M. Chang (2003), Storm track variations as seen in radiosonde observations and reanalysis data, *J. Clim.*, *16*, 480–495.

Hu, Q., Y. Tawaye, and S. Feng (2004), Variations of the Northern Hemisphere atmospheric energetics: 1948–2000, *J. Clim.*, *17*, 1975–1986.

Kalnay, E., et al. (1996), The NCEP/NCAR 40-year reanalysis project, *Bull. Am. Meteorol. Soc.*, *77*, 437–471.

Kanamitsu, M., et al. (2002), NCEP-DOE AMIP-II reanalysis (R-2), *Bull. Am. Meteorol. Soc.*, *83*, 1631–1643.

Krueger, A. F., J. S. Winston, and D. A. Haines (1965), Computation of atmospheric energy and its transformation for the Northern Hemisphere for a recent five-year period, *Mon. Weather Rev.*, *93*, 227–238.

Lorenz, E. N. (1955), Available potential energy and the maintenance of the general circulation, *Tellus*, *7*, 157–167.

Oort, A. H. (1983), Global atmospheric circulation statistics, 1958–1973, *NOAA Prof. Pap. 14*, pp. 180–226, U.S. Gov. Print. Off., Washington, D. C.

Oort, A. H., and J. P. Peixoto (1974), The annual cycle of the energetics of the atmosphere on a planetary scale, *J. Geophys. Res.*, *79*, 2705–2719.

Oort, A. H., and J. P. Peixoto (1976), On the variability of the atmospheric energy cycle within a 5-year period, *J. Geophys. Res.*, *81*, 3643–3659.

Peixoto, J. P., and A. H. Oort (1974), The annual distribution of atmospheric energy on a planetary scale, *J. Geophys. Res.*, *79*, 2149–2159.

Sheng, J., and Y. Hayashi (1990), Observed and simulated energy cycles in the frequency domain, *J. Atmos. Sci.*, *47*, 1243–1254.

Trenberth, K. E. (1991), Storm tracks in the Southern Hemisphere, *J. Atmos. Sci.*, *48*, 2159–2178.

Uppala, S. M. (2001), ECMWF reanalysis, 1957–2001, ERA-40, paper presented at the Workshop on Reanalysis, ECMWF, Reading, U.K., 5–9 Nov.

Uppala, S., et al. (2005), The ERA-40 re-analysis, *Q. J. R. Meteorol. Soc.*, *131*, 2961–3012.

Wiin-Nielsen, A. (1967), On the annual variation and spectral distribution of atmospheric energy, *Tellus*, *19*, 540–559.

D. Feldman, A. P. Ingersoll, X. Jiang, L. Li, and Y. L. Yung, Division of Geological and Planetary Sciences, California Institute of Technology, 1200 East California Boulevard, Pasadena, CA 91125, USA. (liming@gps.caltech.edu)